

## DESIGN AND SIMULATION OF A BLOWDOWN FACILITY FOR SUPERCRITICAL CARBON DIOXIDE

**Mohsen Ghavami**  
ESaNZ Research  
Centre  
City, University of  
London  
London, UK

**Martin T. White**  
Thermo-Fluid  
Mechanics Research  
Centre  
University of Sussex  
Falmer, UK

**Hicham Chibli**  
ESaNZ Research Centre  
City, University of London  
London, UK

**Abdulnaser I. Sayma**  
ESaNZ Research Centre  
City, University of London  
London, UK

### ABSTRACT

*This paper describes an experimental blowdown facility designed to characterise the expansion of supercritical CO<sub>2</sub> near the critical point. Specifically, the test rig aims at replicating the expansion process at the leading edge of a CO<sub>2</sub> compressor with the goal of studying the role of real-gas effects, and possible condensation. The test rig consists of two pressure vessels (high and low pressure), a reciprocating compressor used for charging, a temperature-controlled water circuit to adjust the temperature of the high-pressure tank and a test section comprised of a convergent-divergent nozzle.*

*The specification of the pressure vessels and the recharging compressor is described which are selected to allow for reasonable charging and blowdown times. The design of a thermal management system is also described that keeps the conditions within the high-pressure vessel temperature within the desired range, whilst avoiding over pressurisation. The optimisation of the test rig layout is also discussed which includes identifying an economically and technically viable solution for the positioning of pressure relief valves and the ventilation system. Furthermore, the range of anticipated test conditions that can be achieved and the expected expansion process within the nozzle have been explored using transient lumped mass models of pressure vessels that are coupled with a quasi-steady nozzle model to determine the expected conditions within the nozzle. The nozzle model assumes a homogeneous mixture under thermal equilibrium at any point where the working fluid enters the saturation dome.*

*For the defined test rig specifications (high pressure tank = 0.1 m<sup>3</sup>; low pressure tank = 0.185 m<sup>3</sup>; CO<sub>2</sub> charge = 100 kg; nozzle throat = 100 mm<sup>2</sup>) it is predicated that constant inlet pressure conditions can be sustained for between 0.4 and 5.5 seconds for test section inlet conditions ranging between 27 and 45 °C, and 70 and 90 bar.*

Keywords: supercritical CO<sub>2</sub>, waste heat recovery, non-equilibrium effects, real-gas effects, turbomachinery

### NOMENCLATURE

$b$	nozzle width, m
$C$	cost function, £
$C_B$	base cost for pressure vessel, £
$F_M$	material factor
$L$	nozzle length, m
$\dot{m}$	mass flow rate, kg/s
$M_{\text{charge}}$	total charge of system, kg
$o$	nozzle height, m
$P$	pressure, Pa
$\dot{Q}$	heating/cooling power, J/s
$t$	time, s
$u$	internal energy, J/kg
$V$	volume, m <sup>3</sup>
$W$	weight, kgf
$\rho$	density, kg/m <sup>3</sup>

#### Subscripts

amb	ambient
HP	high pressure vessel properties
LP	low pressure vessel properties
th	throat data

### 1. INTRODUCTION

Waste heat recovery (WHR) offers a significant potential to address energy concerns related to climate change and energy efficiency. For example, it has been estimated that over half of primary energy that is consumed globally is eventually lost to the environment in various forms [1]. Therefore, technologies to capture and convert this waste heat into useful energy are critical.

Within this remit, conversion to electricity remains a viable option since electricity is dispatchable and can easily be transported.

The supercritical CO<sub>2</sub> (sCO<sub>2</sub>) cycle offers very attractive characteristics including high density, chemical stability, reduced compressor work, low global warming potential (GWP), and zero ozone depleting potential that make them ideal for next-generation renewable and WHR power generation applications. Marchionni et al. [2] provided a comparative picture for sCO<sub>2</sub> power cycles against other conventional heat to power systems. Traditionally, steam Rankine Cycle-based power plants can utilise heat sources in a range of 250 °C to 700 °C. However, they are economically attractive only for medium to large heat waste potential [3] as the component efficiencies decrease with reducing size. Organic Rankine cycle (ORC) systems are more suitable in lower power ranges, but are limited to temperatures up to 400 °C because of the limitations related to their working fluids such as flammability and thermal stability. In comparison, sCO<sub>2</sub> WHR cycles have the potential to utilise waste heat in a broad temperature range from 250 °C to 850 °C with power ranging from few hundred kilowatts to 100 MW with efficiencies comparable to or exceeding that of steam Rankine cycles. The techno-economic assessment of sCO<sub>2</sub> power cycles for WHR has found split heating of the flow after compression as being able to generate higher net power compared to other sCO<sub>2</sub> cycle layouts [4]. Simple recuperated sCO<sub>2</sub>, which is the least complex among other sCO<sub>2</sub> cycles, turns out to be the most cost-effective for WHR applications with a specific cost of 770 \$/kW<sub>e</sub> and a payback period of 1.86 years.

Among many challenges that still need to be overcome, the development of suitable turbomachinery designs for sCO<sub>2</sub> power cycles remains a hurdle. These hurdles vary from practical challenges to more fundamental challenges. The former correspond to mechanical, rotodynamic and material challenges related to the high operating temperatures and pressures, and high power-density which means trade-offs between aerodynamic performance and mechanical constraints need to be met. The latter corresponds to improving the understanding of the behaviour of CO<sub>2</sub> under supercritical operating conditions and near the critical point, where non-ideal compressible fluid dynamic and multi-phase effects may occur. Of particular interest is possible phase change in sCO<sub>2</sub> compressors operating near the critical point, which is a concern due to possible condensation. Some studies indicate that the local expansion at the impeller leading edge can exceed 30% of the overall compressor enthalpy rise [5]. Several studies have been carried out to assess two-phase flow in sCO<sub>2</sub> compressors. This includes numerical simulations [6] [7], alongside investigations of non-equilibrium condensation in converging-diverging nozzles [8] [9] [10]. The latter used a blowdown facility where optical visualisation, shearing interferometry and pressure measurements were used to construct the Widom line, and to assess the likelihood of droplet formation based on proximity to the critical point. CFD simulations of cavitating and condensing CO<sub>2</sub> flows have also been conducted using mixture and barotropic models [11], which were used to study sCO<sub>2</sub> compressors [12] [5]. A transcritical refrigeration loop is also under construction to study sCO<sub>2</sub> flows [13].

However, despite these recent advances in the study of condensation in sCO<sub>2</sub> compressors there has yet to be a clear consensus on the role of possible phase change on compressor performance, alongside the development of suitable modelling and simulation tools that have been validated through experimental tests. To address this, there is a need for a coherent set of experimental facilities that can provide the capability to conduct repeatable canonical tests and provide high-quality data for model validation. With this in mind, this paper describes a new test facility under construction at City, University of London that aims to study condensation and non-ideal effects in expanding supercritical CO<sub>2</sub> flows, to provide new insight, whilst supporting the previous investigations mentioned above.

## 2. OVERVIEW OF THE TEST FACILITY

The experimental test rig features a closed-loop blow-down configuration with a test section that can house a nozzle that achieves a specified expansion of sCO<sub>2</sub>. This enables the evaluation of sCO<sub>2</sub> thermo-fluid behaviour in the vicinity of the critical point region; optical and pneumatic measurements will qualify and quantify the phase change of sCO<sub>2</sub> flow inside the test section. The goal is to develop a clear understanding of potential condensation at the suction end of a sCO<sub>2</sub> compressor operating at or below the critical point temperature where compression work is reduced, leading to an improved cycle efficiency. Figure 1 shows a schematic view of the proposed experimental facility.

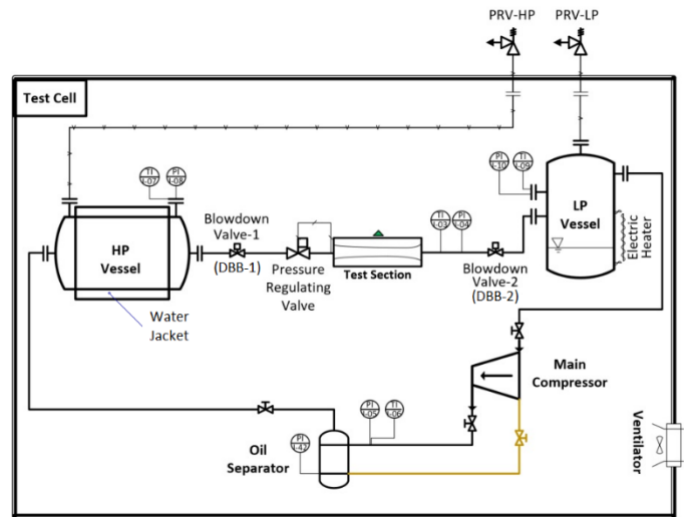


**FIGURE 1:** Schematic of the sCO<sub>2</sub> blowdown test rig.

The test facility will hold a fixed charge of CO<sub>2</sub>, specified at 100 kg and housed in two pressure vessels. A high-pressure tank rated at 130 bar with 100 litre capacity is connected to the upstream of the test section, while a low-pressure tank rated at 75 bar with 185 litre capacity is situated downstream of the test section. Two double block and bleed (DBB) valves tasked with isolating the test section from the upstream and/or downstream components are located on either side of the latter. Each of those valves consist of one manual and one automatic remotely operated

valve with a relief valve between them to avoid over pressurisation of any residual fluid between the two main valves. To simplify the schematic in Figure 1, the DBB valves are shown simply as a single blowdown valve next to each of the pressure vessels.

To regulate the flow through the test section, an additional dome type regulating valve is located between the high-pressure tank and the nozzle. The dome type pressure regulating valves are spring loaded with a short stem and don't use any pneumatic booster. As such they act much faster than most typical pressure regulating valves and their impact on the response time is minimised. A similar arrangement has been used within other blowdown test facilities [10] [14]. The control procedure for the starts from assuming equilibrium in both vessels, as operates as follows: firstly, blowdown valve-1 is shut while blowdown valve-2 is open, and the compressor and HP water jacket is used to charge the system and reach the target conditions in the HP vessel. The blowdown then starts after the conditions in the HP vessel and LP vessel are steady and stabilised with both blowdown valves shut. The blowdown test then starts by opening blowdown valve-1 which applies a pressure upstream of the pressure regulator and causes the valve to move to the set point position. The blowdown valve-2 opens the line after a very short delay and the blowdown process through the nozzle starts.

**TABLE 1:** Key test rig specifications.

Parameter	Value
HP Vessel volume and max pressure	100 litre, 130 bar
LP Vessel volume and max pressure	185 litre, 75 bar
Maximum Temperature	60 °C
Compressor displacement	4.60 m <sup>3</sup> /h
Nozzle Throat Area	100 mm <sup>2</sup>
Nozzle's upstream pressure	80 – 100 bar
Mass Flow Rate (blowdown)	2.8 – 7.5 kg/s

The high-pressure tank is designed with a water-jacket that allows the accurate control of the CO<sub>2</sub> temperature by heating or cooling as required. The low-pressure tank is equipped with a jacket electric heater to provide heating to prevent cooling of CO<sub>2</sub> while emptying the tank. It is connected to the high-pressure tank via a reciprocating compressor that is used to build the required pressure in the high-pressure tank. To remove any oil and other impurities in the CO<sub>2</sub> circuit, an oil separator is also connected downstream of the compressor. Maintaining prescribed hot and cold flows in the water jacket of the high-pressure vessel is done via a separate secondary circuit that uses a chilled water supply coupled with a heat exchanger and dedicated electric heater. The flowrate and temperature of water is controlled to achieve the appropriate final temperature in the high-pressure tank.

The low and high-pressure tanks are both connected to pressure relief valves (PRV) that protect against over-pressurisation of the vessels. These valves provide a safe passage

to release the charge to the outside environment, via two dedicated pipelines that lead from the tanks in the basement level to the PRV's located on the roof of the building.

### 3. TEST RIG MODELLING

The modelling of the test rig includes individual models each of which serve certain purposes. A transient model has been developed to establish the relation between the characteristics of the charging and discharging processes and the component specifications, particularly the size of the pressure vessels and the compressor. A quasi-steady quasi-1D nozzle model is used to predict expected flow conditions in the nozzle. This nozzle model is integrated in a full system model to study the flow conditions in the test section during the blowdown process.

#### 3.1. Transient lumped mass model

The modelling assumes a fixed CO<sub>2</sub> charge and a set target pressure and temperature for the HP tank. At the start of the charging process, it is also assumed that the test rig is at thermal equilibrium with the ambient surroundings and that both the HP and LP tanks are at equilibrium. Therefore, the initial pressure and density within both tanks is dictated by the total charge, total test rig internal volume and the ambient temperature, since  $\rho = M_{\text{charge}} / (V_{LP} + V_{HP})$  and  $P = f(\rho, T_{\text{amb}})$ . The model assumes bulk properties are constant within each tank and there is no heat loss to the surroundings. The modelling of the charging process is depicted in Fig. 2. To determine the bulk properties within each tank during charging, the lumped-mass conservation laws for each tank can be formulated as follows:

$$\frac{d(\rho_{HP}V_{HP})}{dt} = \dot{m} \quad (1)$$

$$\frac{d(\rho_{LP}V_{LP})}{dt} = -\dot{m} \quad (2)$$

$$\frac{d(\rho_{HP}V_{HP}u_{HP})}{dt} = \dot{m}h_{comp} + \dot{Q}_{HP} \quad (3)$$

$$\frac{d(\rho_{LP}V_{LP}u_{LP})}{dt} = -\dot{m}h_{LP} + \dot{Q}_{LP} \quad (4)$$

where  $\rho$ ,  $u$  and  $V$  correspond to the bulk fluid density, bulk internal energy and tank volume respectively, while the subscripts HP and LP refer to the high- and low-pressure tanks. The term  $\dot{m}$  is the mass-flow rate displaced by the compressor, which is in turn related to the compressor swept volume and the rotational speed, assuming a reciprocating piston compressor. The enthalpy leaving the compressor,  $h_{comp}$ , is calculated based on the assumption of an isentropic compression efficiency of 65% acting across the pressure difference between the two tanks. Finally,  $\dot{Q}_{HP}$  and  $\dot{Q}_{LP}$  correspond to the heating or cooling load provided by the jacket water to the HP tank, and heating load on the LP tank respectively. The heating or cooling load on the HP is input as a fixed heat load (i.e., fixed kW), rather than being modelled with a more detailed heat transfer model that accounts for the flow rate of cooling water,

the heat transfer coefficients for the water and within the HP vessel, and the heat transfer area. The reason for this is because the heat transfer rate will only influence the resulting charging time which is of secondary importance and as such an order of magnitude prediction is sufficient. For example, it is envisioned that two to three test runs might be completed in one day, and therefore a charging time ranging anywhere between 10 minutes to an hour would be considered acceptable. The heating load on the LP tank is also input as a fixed heat load and is a simple representation of the total heat supplied to the LP tank via the electric heater and heat transfer from the surroundings. Without the addition of this heat load in the model, the predicted temperature within the LP tank would drop below 0 °C due to removal of mass and energy.

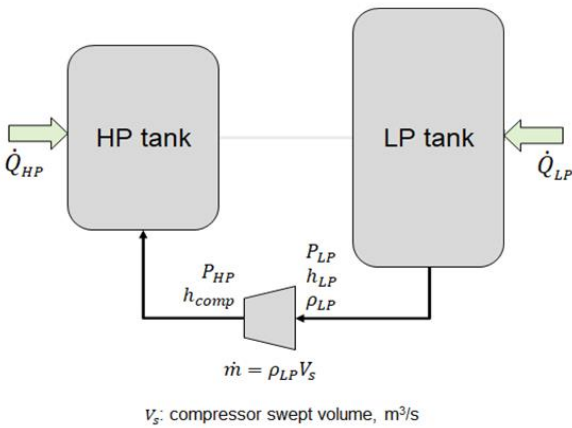


FIGURE 2: Schematic of the test rig charging process.

The solution to Equations (1)-(4) is obtained using a finite difference scheme that starts from  $t = 0$  and marches forward in time. Within the model, binary flags are setup to turn the compressor and heating on and off independently to reach the target HP tank conditions without leading to excessive pressures in the HP tank.

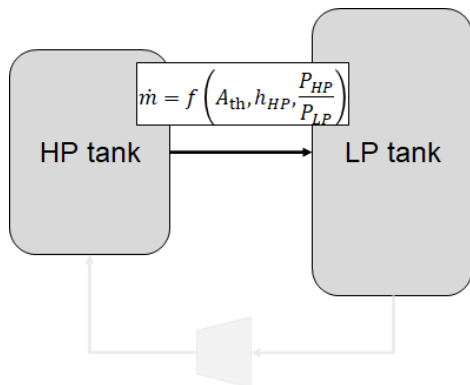


FIGURE 3: Schematic of the blowdown process.

Similarly, the modelling of the blowdown process is shown in Fig. 3. The blowdown modelling assumes initial HP and LP tank conditions after charging and the simulation is run until

pressure equilibrium is achieved ( $P_{HP} = P_{LP}$ ). The blowdown time is the time taken to reach this equilibrium condition.

As with the charging process, the bulk properties within each tank are obtained a similar set of conservation laws:

$$\frac{d(\rho_{HP}V_{HP})}{dt} = -\dot{m} \quad (5)$$

$$\frac{d(\rho_{LP}V_{LP})}{dt} = \dot{m} \quad (6)$$

$$\frac{d(\rho_{HP}V_{HP}u_{HP})}{dt} = -\dot{m}h_{HP} \quad (7)$$

$$\frac{d(\rho_{LP}V_{LP}u_{LP})}{dt} = \dot{m}h_{HP} \quad (8)$$

where all parameters have the same definition as before. The mass-flow rate  $\dot{m}$ , is calculated based on a defined nozzle throat area (i.e., the minimum area in the test section), and a specified target test section inlet stagnation pressure, denoted  $P_0$  which is maintained by a pressure regulating valve installed between the HP tank and the test section. The pressure regulation valve is modelled simply by considering an expansion from  $P_{HP}$  to the target test pressure  $P_0$  that is isenthalpic (i.e.,  $h_0 = h_{HP}$ ) in the case that the HP tank is higher than the target test section inlet pressure. In the case that the pressure regulation valve is fully open (i.e., when  $P_{HP}$  is lower than the set pressure), then  $P_0 = P_{HP}$ . The mass-flow rate is then calculated based on the pressure difference between  $P_0$  and  $P_{LP}$ . If the pressure difference exceeds the critical pressure ratio then the nozzle is assumed to be choked and the mass-flow rate is set based on the choked flow conditions and the throat area assuming isentropic expansion from the test section inlet conditions (i.e.,  $\dot{m} = \rho^* a^* A_{th}$ ). Otherwise, the mass-flow rate is determined based on an isentropic expansion from the test section inlet conditions to the LP pressure and a defined nozzle outlet area. It should be noted that the upstream pressure of the test section (i.e. upstream pressure of the nozzle) will be kept fixed using the pressure regulating valve. Therefore, despite the impact of the blowdown (DBB-1) valve, the mass-flow rate can be estimated using the upstream pressure and temperature, downstream pressure and the nozzle dimensions.

### 3.2. Quasi-steady quasi-1D nozzle model

A quasi-steady quasi-1D inviscid model has been developed to design the nozzle and estimate the flow conditions within the nozzle for any prescribed set of boundary conditions. The assumption of quasi-steady flow within the nozzle is rationalised due to the short residence time of the flow within the nozzle compared to the timescale of variations in the tank conditions. As a preliminary approximation, it is assumed that any regions of two-phase flow can be treated as a homogeneous mixture of liquid and vapour at thermal and mechanical equilibrium. This means that both the liquid and vapour remain at the same temperature, and pressure, which corresponds to the saturation conditions, and travel at the same velocity. Subsequently, the mixture can be treated as a single fluid, which means that a single set of

conservation laws govern the two-phase mixture, and the fluid behaviour is analogous to a single-phase vapour. As such conventional nozzle theory can be applied to predict fluid behaviour inside the nozzle, including the prediction of normal and oblique shocks within the nozzle or at the outlet of the nozzle, as long as the conservation laws are coupled with an appropriate equation of state. The assumption of homogeneous flow under mechanical equilibrium is motivated by the proximity to the critical point, which means the difference in density between the liquid and vapour phases is small, while surface tension effects are diminished. The assumption of thermal equilibrium is likely to be an oversimplification, but is considered to be a suitable assumption for the purposes of this current paper which is focussed on specifying the main components of the test rig, and assessing the achievable testing times. However, more detailed non-equilibrium CFD simulations are currently underway which will ultimately be compared to results from experimental tests.

The nozzle is initially designed for a specific set of boundary conditions, defined in terms of an inlet stagnation pressure and temperature, inlet velocity, mass-flow rate and static outlet pressure. Under the assumption of thermal and mechanical phase equilibrium, the flow conditions within the nozzle can be easily determined assuming an isentropic expansion. Thus, an array of static pressure values ranging from the inlet static pressure (calculated based on the specified inlet velocity) to the static outlet pressure is constructed and the corresponding arrays of velocity and density, and subsequently flow area are constructed. This area array is mapped across to a physical nozzle geometry by defining the target static pressure distribution as a model input, which is defined using a Bezier curve with 3-control points, as described in a previous publication [15]. The final geometrical parameters of the nozzle are defined by two non-dimensional design inputs which define the length of the nozzle  $L$ , and the nozzle passage width  $b$ , as a fraction of the nozzle throat height  $o_{th}$  (i.e.,  $b/o_{th}$  and  $L/o_{th}$ ). As noted, the nozzle design tool is based on a quasi-1D approach, and therefore 2D effects within the nozzle are neglected. This is considered appropriate for two reasons. Firstly, the focus of the current study is on the subsonic flow upstream of the throat, and thus 2D flow patterns, such as expansion fans in supersonic flow that require a 2D design method such as the method of characteristics are not present. Secondly, this study is not concerned with optimising the geometry of the nozzle, but rather studying fundamental aspects related to expanding supercritical CO<sub>2</sub> flows in a representative geometry. In this context, as long as the geometry of the nozzle is consistent in both the experiment and resulting CFD simulations, then meaningful results can be expected.

With the nozzle geometry fixed, the model is also able to provide an estimation for the streamwise variation in pressure, velocity, temperature, and vapour quality along the length of the nozzle for any given set of inlet stagnation conditions and static outlet pressure. Thus, by coupling the quasi-1D nozzle model with the transient lumped-mass model it is possible to predict the flow conditions within the nozzle at different points during the blowdown process. The calculation process adopted by the model can be summarised as follows:

1. In the first instance, based on the specific stagnation inlet conditions and nozzle throat area, the choked mass-flow rate is calculated. If the mass-flow rate is lower than the choked mass-flow rate, then the nozzle is entirely subsonic and the flow conditions at each location within the nozzle can be obtained by an iterative mass-balance assuming isentropic expansion to derive the static properties and velocity.
2. If the nozzle is choked, the next step is to determine the range of static outlet pressures for which a normal shock is expected to form within the nozzle. The maximum and minimum static outlet pressures correspond to the situations where a normal shock forms at the throat and the nozzle outlet respectively, and these can be found by assuming isentropic expansion up until the shock location, and then iteratively solving the normal shock relations to determine the downstream conditions.
3. If the static outlet pressure lies between these limits, then a normal shock occurs within the nozzle. An iterative method is then adopted to find the location of the normal shock that corresponds to the defined outlet pressure. To determine the fluid properties and velocity upstream and downstream of the shock, an iterative mass-balance assuming isentropic flow either side of the shock is then applied.
4. If the static outlet pressure is below the minimum pressure that corresponds to a normal shock within the nozzle, then the flow is over-expanded and an oblique shock forms downstream of the nozzle outlet, or the flow is under-expanded. In either of these cases, the flow conditions within the nozzle are found assuming isentropic expansion within the nozzle itself.

## 4. TEST RIG DESIGN AND SIZING

### 4.1. Parametric study for component sizing

The lumped mass model introduced in Section 3.1 has been used to carry out parametric studies. The objectives of the parametric studies are to evaluate the optimum CO<sub>2</sub> charge, the pressure vessel volumes, the thermal (heating and cooling) loads on each of the pressure vessels and the blowdown time. These studies are done for several compressor volume flow rates, thermal loads and an upper limit for the cost of the vessels.

The cost of the pressure vessels is a function of maximum allowable working pressure (MAWP), volume and the material used. The MAWP is ultimately decided by the upper limit of the desired pressure range upstream of the test section and the pressure difference across the pressure regulating valve. As the test section is expected to operate with a transcritical expansion process, the target range of stagnation pressures upstream of the test section are set to be within the range of 80 bar to 100 bar. The pressure upstream of the pressure regulating valve thus needs to be greater than 100 bar to establish the flow for different test conditions. A parametric study concerning the size of the two pressure vessels has been done for a maximum pressure range of 115 bar to 145 bar. The estimation of the base cost for the pressure vessels is based on the evaluation of the weight as defined by equations (9) and (10) for the horizontal and vertical pressure vessels

respectively [16]. In these equations, the base cost  $C_B$  is calculated in USD and  $W$  is the weight of the pressure vessel in kgf. The final cost is calculated using equation (11) where  $F_M$  is the material factor which is set to 1.7 since the HP and LP pressure vessels will both be made from stainless steel:

$$C_B = e^{\{8.717 - 0.23320 \ln(2.2W) + 0.0433(\ln(2.2W))^2\}} \quad (9)$$

$$C_B = e^{\{6.775 + 0.18255 \ln(2.2W) + 0.02297(\ln(2.2W))^2\}} \quad (10)$$

$$C_{vessel} = F_M C_B \quad (11)$$

The weight of the pressure vessel is evaluated based on the material strength, the allowable mechanical stresses for the chosen material and the dimensions. The aspect ratio of the high pressure and low-pressure vessels have been assumed to be between 3 to 5. Moreover, the arrangement of the test rig in the available space dictated that the high-pressure vessel has a horizontal arrangement whilst and the low-pressure vessel will be standing vertically. Figure 4 shows the variation in the tank volumes for different maximum pressure ratings. The total cost is fixed at 40,000 GBP as per the allocated budget for the manufacturing of the pressure vessels. The final choice of the high pressure and low pressure vessels was done considering the charging and blowdown times, as discussed in the following paragraphs. As Figure 4 demonstrates, it is possible to stay within the budget with a very small HP vessel and very large LP vessel or vice versa. However, correct sizing is only achievable when considering the charging and blowdown processes with a certain maximum pressure. The maximum pressure is selected based on the technical limits dictated by the available compressor technology.

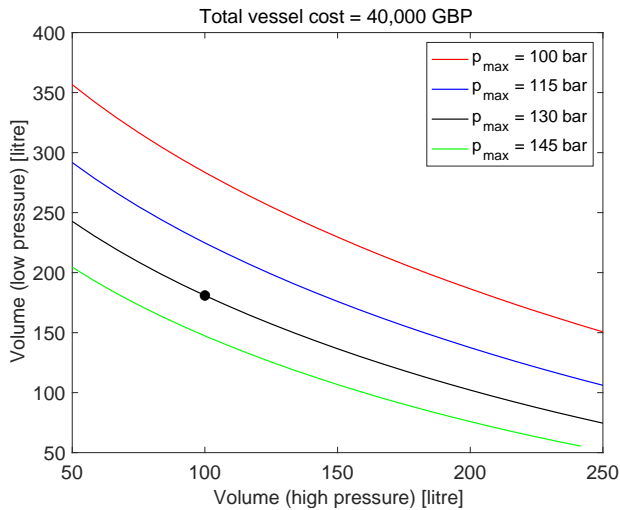


**FIGURE 4:** Possible HP and LP tank sizes based on different rated pressures assuming a fixed budget of £40,000.

The recovery compressor is used for charging the high-pressure vessel after each test. The choice of the compressor is mainly dependent on its performance envelop. As the application of transcritical CO<sub>2</sub>-based refrigeration systems has grown, the technology of the transcritical compressors has become more

mature. However, the range of working pressure of such compressors is still limited. The compressor which is chosen for the test rig is BOCK, HGX24/55-4 SH which is a reciprocating transcritical compressor capable of compressing carbon dioxide in supercritical conditions to pressures as high as 130 bar as shown in Figure 5. The minimum and maximum operating temperatures with CO<sub>2</sub> as the working fluid for the compressor are 5 °C and 85 °C respectively. The minimum temperature is for the suction side and the maximum temperature is given for the discharge of the compressor.

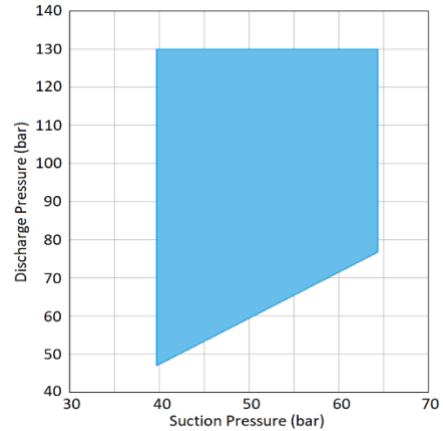


**FIGURE 5:** Working pressure range of the compressor.

It is worth noting that the compressor used for charging the LP vessel is a positive displacement reciprocating machine and the variations in its volumetric efficiency with pressure is not as significant as for non-positive displacement machines. Here, a fixed volumetric efficiency has been assumed. Although in practice, the volumetric efficiency may slightly decrease under high discharge pressures, the dynamics of the compression process are not critical to this study.

The variations in the properties of CO<sub>2</sub> in the HP and LP vessels are predicted using the transient lumped mass model for a target test pressure and temperature. An example of the predictions obtained from the model for the charging and blowdown processes are shown in Figure 6 and Figure 7. The results are generated assuming the target test stagnation pressure of 100 bar and stagnation temperature of 35 °C. During the charging process, the compressor draws the fluid in the low-pressure vessel and transfer it to the high-pressure vessel. As a result, the pressure and temperature will be increased in the HP vessel while in the LP vessel the pressure and temperature will drop. The changes in pressures are the desired outcome of the charging process. However, thermal management in the HP and LP vessels is required to maintain the fluid temperature within a reasonable range. In the first instance, the temperature range must observe the maximum and minimum temperature limits of the compressor. Keeping the HP temperature as low as possible during the charging will also help to reduce the charging time and ensure efficient operation of the compressor. Moreover, a degree of thermal management is also necessary to achieve the desired test

temperature. The results in Figure 6 indicate that the charging process requires alternating compression and cooling stages to reach the required pressure and temperature in the HP vessel.

The charging process shown in Figure 6 takes a total of 30 minutes to reach the target conditions. However, the time it takes to charge the system is dependent on both the compressor displacement and the cooling rate. As noted in Section 3.1, a charging time under an hour is considered sufficient to enable several test runs to be completed within a day.

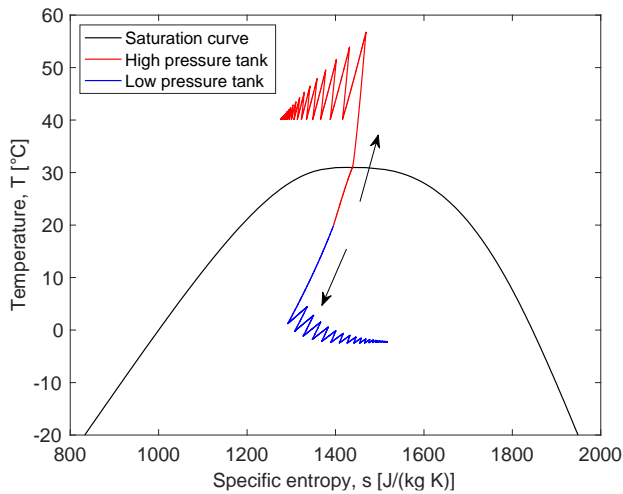


**FIGURE 6:** Variations of CO<sub>2</sub> properties in high pressure and low-pressure tanks during charging process;  $M_{\text{charge}} = 100 \text{ kg}$ ;  $\dot{Q}_{\text{HP}} = -5 \text{ kW}$ ;  $\dot{Q}_{\text{LP}} = 3 \text{ kW}$   $V_s = 2 \text{ m}^3/\text{hr}$ . The arrows indicate the direction of the evolution of the tank properties during charging.

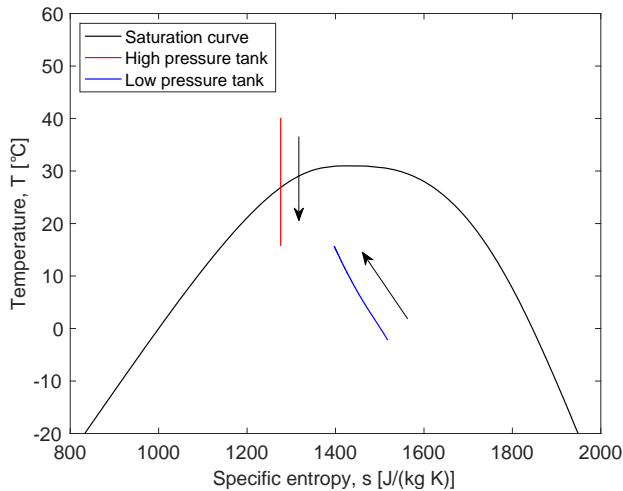


**FIGURE 7:** Variations of CO<sub>2</sub> properties for the blowdown process, following charging according to Fig. 6. The arrows indicate the direction of the evolution of the tank properties as the blowdown process progresses.

Ultimately, Figure 6 demonstrates how the charging process results in the temperature rise of the fluid in the HP vessel, which subsequently requires cooling of the tank. The sizing of the

compressor determines the rate of mass, and energy input to the HP tank over time, and thus the required cooling rate is dependent upon the compressor displacement. To assess the relationship between these two control parameters a parametric study has been conducted considering different compressor displacements and cooling loads. For this study, for each pair of values for the compressor displacement and cooling load the resulting tank temperature is determined following a charging process that involves running both the compressor and cooling water continuously until the maximum pressure of 130 bar is achieved. The tank volumes and CO<sub>2</sub> charge remain constant. The results are reported in Figure 8, which show how the temperature in the HP vessel decreases more rapidly with the cooling power for a smaller charging flow rate. Ultimately, these results show that to reach a specific temperature, precise control over the cooling load, such that the temperature drop caused by the cooling water is equal to the temperature increase caused by the compressor, would be necessary. However, the implementation of such a control system was deemed unnecessary since precise control of the charging process is not critical. Instead, the charging involves periods of charging, during which the pressure and temperature in the HP vessel increases, followed by a period when the compressor is switched off and the cooling provided through the water jacket reduces the temperature of the tank. This is necessary to ensure operating temperatures remain at a safe level for the compressor and pressure vessels, whilst ensuring the target conditions are met. The cooling system operates continuously throughout the charging process, but the compressor is periodically switched on and off until the target conditions are reached.

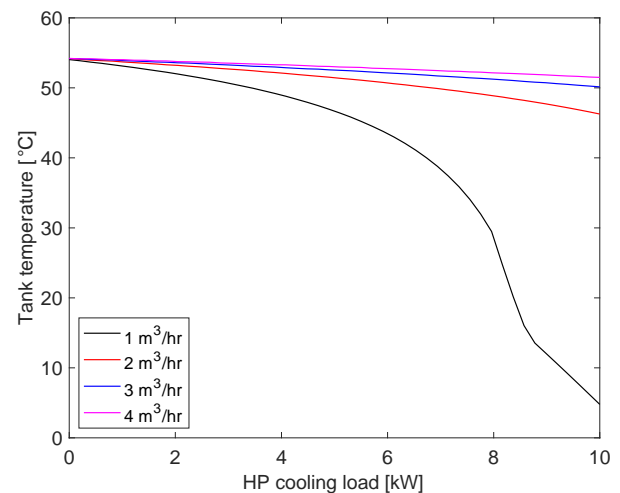


**FIGURE 8:** Parametric study showing the resulting HP tank temperature for different compressor displacements and HP tank cooling load. Target pressure is set to 130 bar.

During the blowdown process, the compressor will be isolated by its inlet and outlet valves and the automatic valves in the blowdown line will open and CO<sub>2</sub> expands from the HP tank to the LP tank through the nozzle. The blowdown continues until the two tank pressures equilibrate, as shown in Figure 7. Referring

to this figure it can be noted that after charging, and at the beginning of the blowdown process, the conditions within the LP tank are slightly below 0 °C. This is linked to the assumed heat load on the LP tank during charging, which is only roughly approximated, and the fact that the blowdown process starts immediately after charging has completed. However, additional heating from the electric heater, or heat transfer from the surroundings would likely lead to the LP tank approaching the ambient temperature before the blowdown process is initiated.

From the transient model of the blowdown process it is possible to determine the blowdown time. The main parameters that influence the time for blowdown are the size of the HP vessel that holds the charge before blowdown, the size of the LP vessel, and the total amount of the CO<sub>2</sub> charge. This is alongside the size of nozzle throat which determines the amount of mass-transfer between the tanks. The maximum pressure in the HP vessel also affects the blowdown time and is assumed to be 130 bar as discussed above. Figure 9 reports results from a parametric study considering the variation of the blowdown time with the total volume of the HP vessel for different amount of CO<sub>2</sub> charge in the tank. In this study, for each HP tank volume the LP tank is sized such that the total cost of the HP and LP tanks is equal to the total budget available, whilst a fixed nozzle area of 100 mm<sup>2</sup> is assumed. Here, the blowdown time is defined as the total time for the pressures in the HP and LP tanks to equilibrate. These results show that a larger tank volume, and a lower charge is beneficial to maximise blowdown time since this maximises the total mass stored in the HP tank, whilst minimising the mass and pressure of the LP tank. The discontinuities observed for higher charges are related to the initial LP tank conditions, which can either be in the superheated vapour or two-phase region.

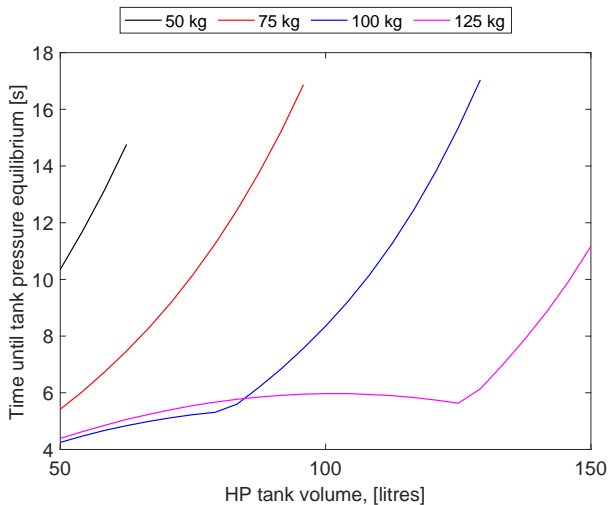


**FIGURE 9:** Parametric study reporting the time it takes for the HP and LP tanks to reach pressure equilibrium during the blowdown for different HP tank volumes and CO<sub>2</sub> charge. Target test conditions of 100 bar and 35 °C.

## 4.2. PRV arrangements

The existence of high pressure CO<sub>2</sub> in the test rig requires pressure relief valves (PRV) to protect the test rig from unintended over-pressurisation above the strength of the components. Given that the test rig has a high-pressure side, rated at 130 bar and a low-pressure side, rated at 75 bar, it is required that the test rig uses two separate PRVs with different pressure settings.

The main concern with the use of PRVs for the test rig was that it is located at the basement of the university’s building which has access to a common exhaust tunnel working at a relative negative suction pressure. Normally, the PRVs are just mounted on top of the pressure vessels and discharge the excess pressure to the ambient. However, that is not an option when using CO<sub>2</sub> due to its asphyxiation hazard. Furthermore, the discharge of CO<sub>2</sub> from the PRVs to long pipes etc. to direct the flow out of the building is also dangerous because of the high risk of dry ice formation. The dry ice can form in a pipe where the pressure is below the triple point pressure at 5.18 bar. As such, the regulations require that the discharge of the PRV must not be connected to any piping line. That meant positioning of the PRVs outside of the building and installation of the piping between the pressure vessels and the inlet of the PRVs.

To optimise the cost and operation of the PRVs, a few design scenarios were considered including over rating the LP vessel to 130 bar similar to the HP side and adding a large buffer tank to allow the PRV of the HP side to discharge to a lower pressure. In either of those scenarios, it was possible to half the amount of piping. However, the technical and economic studies found that two separate PRV would be the optimal solution.

## 4.3. Ventilation

Any potential release of carbon dioxide from the test rig causes an asphyxiation hazard and requires implementation of safety management in relation to the concentration and time of exposure as detailed in the HSE EH40/2005 document under CAS number 124-38-9 [17]. This schedule stipulates that exposure to CO<sub>2</sub> is to be capped to long-term and short-term limits as shown by Table 2.

**TABLE 2:** The exposure time limits for CO<sub>2</sub> as per HSE EH40/2005 [17]

Substance	Workplace exposure limit			
	Long-term exposure limit (8-hr period)		Short-term exposure limit (15min period)	
	ppm	mg/m <sup>3</sup>	ppm	mg/m <sup>3</sup>
Carbon dioxide	5000	9150	15000	27400

The mentioned regulations require the implementation of a ventilation system to allow for keeping the concentration level of CO<sub>2</sub> below the maximum allowable limit in case of any leakage or accident. To assess the ventilation requirements, a numerical study was conducted to simulate the possible scenarios of CO<sub>2</sub> accumulation in the test cell space resulting from of an

uncontrollable release of all or part of the CO<sub>2</sub> charge. Two main categories of events were considered: sudden initial release, and gradual leakage over a time period.

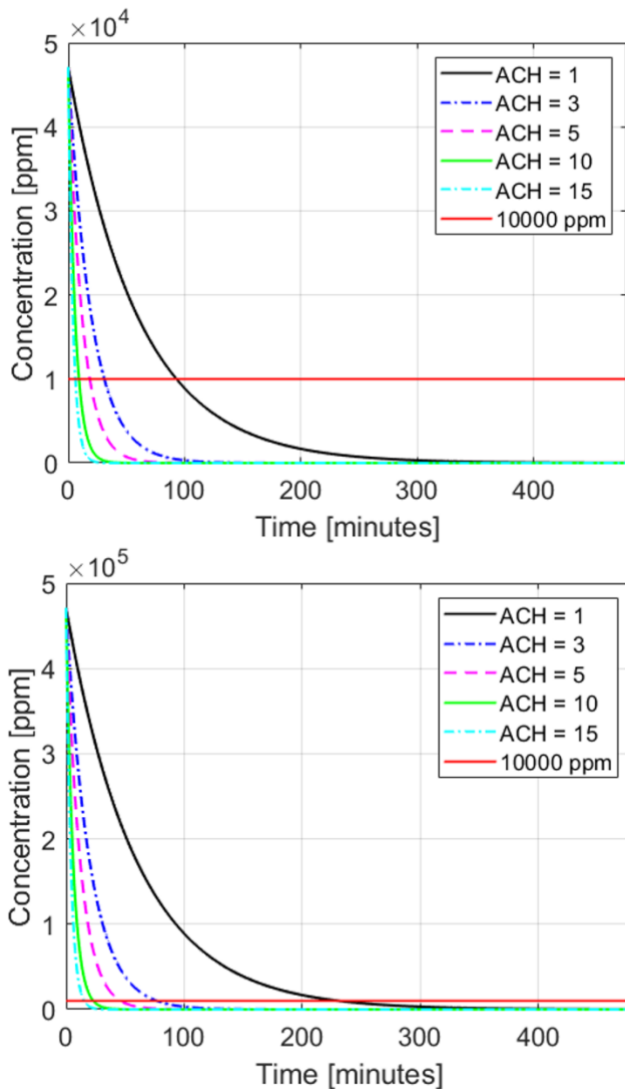


**FIGURE 10:** Concentration of CO<sub>2</sub> following an instant release for 10% (top) and 100% (bottom) of the total charge.

The calculations suggest that a continuous exhaust system capable of delivering 15–45 air changes per hour (ACH) is essential to protect the staff in the lab and the immediate environment in the event of CO<sub>2</sub> buildup. It is noted that the scenarios considered correspond to any catastrophic failures of equipment including pressure vessels, test section, valves, fitting, piping and other hardware that lead to a full or partial discharge of compressed CO<sub>2</sub> instantly or over a period of time. It is assumed that the system contains the full charge of CO<sub>2</sub> (i.e. 100 kg) in the calculations. These results are shown in Fig. 10.

A number of additional safety measures are also in place to mitigate the hazards of potential CO<sub>2</sub> release including a visual indicator at the entrance to the test cell and an audio-visual alarm

system which will be triggered by CO<sub>2</sub> sensors implemented inside the test cell at different positions. The sensors will activate the alarm system as soon as the carbon dioxide level is detected above the allowable limit mentioned before. A flow pressure monitoring system is also integrated to the safety system to ensure the operation of the ventilations fans through the existence of the actual air flow.

#### 4.4. Test section design

The test line corresponds to the piping arrangement that sits between the upstream pressure regulating valve, which controls the stagnation pressure entering the test section, and the LP tank. This section starts with a pipe with a circular cross-section which is connected to a contraction piece. This contraction piece is designed to enable a smooth transition from a flow channel with a circular cross section to a flow channel with a planar cross section that is compatible with the planar test section. This piece should be designed to avoid flow separation, while ensuring a high degree of flow uniformity at the outlet of the contraction. The contraction piece has been designed in accordance with that detailed in a previous publication related to designing a similar component for a test rig designed to examine ORC turbomachinery flows [18].

Immediately after the contraction zone, the flow enters the test section which houses the test nozzle. As the flow passes through the nozzle and expands, the velocity increases and the pressure reduces. Depending on the proximity of the stagnation inlet conditions to the critical point, this acceleration can cause the flow to enter the saturation dome and cause condensation to occur. To design the test section nozzle, the process described in Section 3.2 is followed, with the following design inputs:  $b/o_{th} = 3$ ,  $L/o_{th} = 20$ .

As an initial assessment on the possibility of condensation to occur, the resulting nozzle has been simulated for a fixed inlet temperature of 313 K and at inlet stagnation pressures ranging between 75 and 90 bar. The goal of this analysis is to establish the pressure profile, and more importantly the vapour quality distribution within the nozzle, that might be expected for different stagnation inlet conditions. The results ultimately show that for the four cases evaluated, condensation within the later stages of the nozzle is predicted. However, as noted previously, the homogeneous thermal equilibrium is likely to be an oversimplification, and in reality, any non-equilibrium effects should in theory move the onset of condensation further downstream than predicted here. As such the results indicate the earliest location that the condensation may occur. It is also worth noting that under the equilibrium assumption, there is no length dependence – in other words, if the same nozzle was stretched in the y-direction (but the same non-dimensional pressure profile was maintained) then the variations would look the same, and the relative location of the onset of two-phase effects would be the same. However, looking at different nozzle lengths in the future is also of interest because it allows to investigate how residence time affects the condensation process. The role of non-equilibrium effects, and the length of the nozzle will be studied in subsequent studies that be completed alongside commissioning of the test facility.

The test section assembly embodies the nozzle and contraction pieces providing the flow passage where the flow expansion and pressure drop are expected to take place. At present, the test section housing is not assumed to be heated and therefore at the start of testing the walls of the test section are assumed to be equal to the ambient temperature. Based on a preliminary assessment, the amount of heat transferred from the fluid to the walls as it passes through the test section is estimated to be small. This is due to the very short residence time as the flow passes through the nozzle, and the relatively small temperature difference since the target expansion processes correspond to temperatures near the critical point. However, an assessment of whether any heating is required on the lines connecting the tanks to the test section is currently underway.

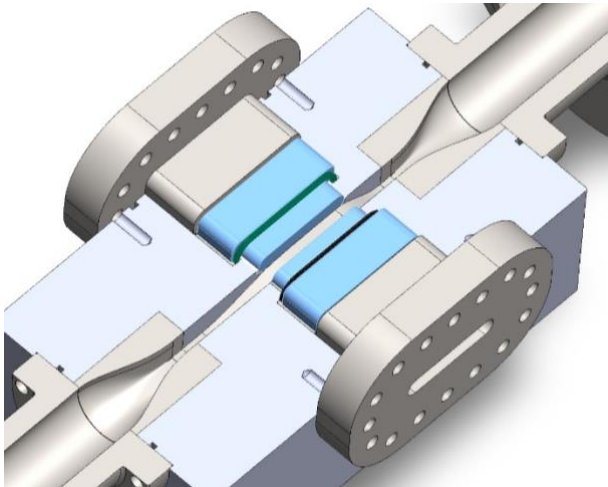


**FIGURE 11:** Test section assembly. Section view from the top with the two glass assemblies (not sectioned).

Figure 11 shows a longitudinal section view of the test section assembly and the flow passage from the top. As it can be seen in Figure 11, the flow passage through the test section starts with the circular cross section followed by the contraction piece which provides smooth transition from the circular cross section to the rectangular cross section of the nozzle's inlet. The nozzle piece defines the shape of the nozzle flow as discussed earlier. The flow will exit the nozzle throat through a diverging section followed by another cross-section transition, similar to the inlet contraction piece. Depending upon the upstream and downstream conditions, the diverging exit section could result in further expansion leading to supersonic flow and shock waves. However, the presence of such effects is not considered to conflict with the objectives of the planned tests which are focussed primarily on subsonic and transonic flows close to choked flow conditions. As such, the conditions upstream of the throat and at the throat will be recorded and used for the calibration and validation of the CFD models.

The flow passage through the nozzle in Figure 11 is constructed with two side glass pieces which are supported by metallic side plates. The glass pieces provide visual access to the flow passage where the nozzle is located and the condensation front is expected. Figure 12 provides a side view to the test section

assembly which is cut along the mid plane of the test section and shows the flow passage. The silhouette of the side plate has been also added to picture to show how the glass sub-assembly provide visual access to the nozzle and the flow passage.

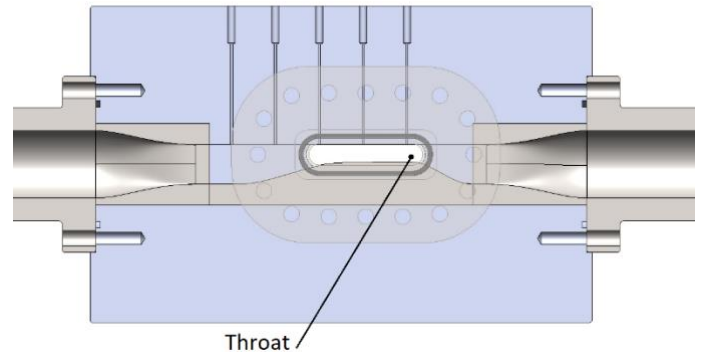


**FIGURE 12:** Side-section view of the test section assembly.

The test section design provides the flexibility to test different nozzle profiles with minimum number of parts replacements. The glass pieces are made from thermally toughened borosilicate glass. To avoid metal to glass contact, a gasket separates each glass piece and its side plate. Given that the test section assembly is a pressurised system under an internal pressure, the design must follow the applicable pressure safety regulations. In the UK, the applicable regulations, PD5500 sets a maximum allowable stress  $f_E$  as per equations (12) and (13), and this is set to the lower of the values predicted. In these equations  $R_e$  and  $R_m$  are the yield and tensile strength of the material respectively. The test section is made from Duplex stainless steel BS 318S13 and the maximum allowable stress is 260 MPa.

$$f_E = \frac{R_e}{1.35} \quad (12)$$

$$f_E = \frac{R_m}{2.5} \quad (13)$$

#### 4.5. Instrumentation

The main properties that will be measured on the test rig are the pressure and temperature at different points as indicated in Figure 1. The pressure transducers are OMEGA MM series which are piezoresistive pressure transducer type. The piezoresistive process uses strain gages embedded into a highly stable silicon wafer making them very robust for the intended application of the test rig. The uncertainty of the sensors is 0.5% of the full scale, which is 150 bar for the HP side and 100 bar for the LP side of the test rig. The temperature sensors are of the Pt-100 RTD (Resistance Temperature Detector) type, which have up to 0.75% error of the reading value in the readout. The RTDs are installed on the HP and LP vessels via thermowells to facilitate their removal for the maintenance or calibration purposes. The same sensors are used for the temperature measurement at the compressor discharge as provided by the manufacturer. The use of RTDs is justified by their accuracy and robustness. The dynamics of temperature change in pressure vessels and charging process are

slow enough to make the RTDs a suitable choice. However, for the temperature measurement in the vicinity of the test section, three T-type exposed tip thermocouples will be used for the purpose of reliability. The exposed tip thermocouples have much faster response than the RTDs.

Incorporating the theoretical blowdown time calculated for different testing conditions (Section 5) and estimated response times of the pressure regulating and solenoid valves that isolate the test section, a measurement window of 100 - 500 ms is anticipated. The test section assembly accommodates five tappings for high sample rate pressure sensors. These sensors can provide 2000 readouts per second with an uncertainty of 0.1% of the full scale, which makes them suitable for capturing the transient effects expected in the flow through the nozzle. The pressure transducers are Kulite ETM-HT-375CO. Since these probes are not flush mounted inside the test section walls (see Figure 12), the dimensions of the tapping holes were selected to avoid inducing a resonant response. A classic lumped mass Helmholtz resonator model was incorporated to characterise the tapping neck and plenum space that hosts the transducer head. This yielded an acoustically compact chamber with a predicted natural frequency of 200-350 Hz for the various flow conditions, with a ratio of physical resonator neck to wavelength of a sound wave at the respective frequencies of 0.41. As Paxton [19] demonstrated using a 1-D acoustic model of a probe mounting chamber with a ratio of neck to wavelength of 1.0, the lumped mass analysis predicted the resonant frequency quite accurately.

The data acquisition system uses an eight slot NI-CompactDAQ cDAQ-9178 with analogue input modules for voltage and current from Kulite and OMEGA transducers respectively and another RTD module for reading the Pt-100 temperature sensors. The data acquisition and data recording is managed using LabVIEW.

#### 4.6. Flow visualisation and optical techniques

The present research aims to build a test rig which among its other objectives is going to be used for characterisation of the condensation of the sCO<sub>2</sub> and for the validation of numerical simulations. As such, the test rig aims to allow for qualitative and quantitative measurement of the condensing flow to allow for the visualisation of the onset of the condensation and measurement of the refractive index gradients. The optical setup will be based on Background Oriented Schlieren (BOS) which can be used to visualise refractive index gradients. The hardware required for BOS includes a high-resolution camera, a lens, and a light source illuminating the background pattern as shown in Figure 13.

The sensitivity of the BOS measurement is improved with a large distance from the flow to the background which offers an advantage for this test rig given the available distance for the test section setup. The spatial resolution depends directly on the resolution of the camera sensor, pixel size, and the field-of-view.

Interferometry has been preferred over Schlieren and background oriented Schlieren in some previous work [9]. However, it is a more complex and relatively more expensive method compared to BOS. Furthermore, there is much experience,

and a wide range of equipment are already available to the research team of the project that can support BOS.

An important aspect of the optical setup discussed for this test rig is that, given the nucleation time and the residence time interval of the flow in nozzle, it will only be possible to see the very beginning of the onset of the nucleation, and hence the droplets will be very small. That would require the use of high-speed lenses that allow maximum possible light to reach the sensor of the high-speed camera. Because of its line-of-light arrangement, BOS also facilitates the use of telescopic lenses that would allow to focus on very small area of the flow for a higher chance of capturing the nucleation of the flow.

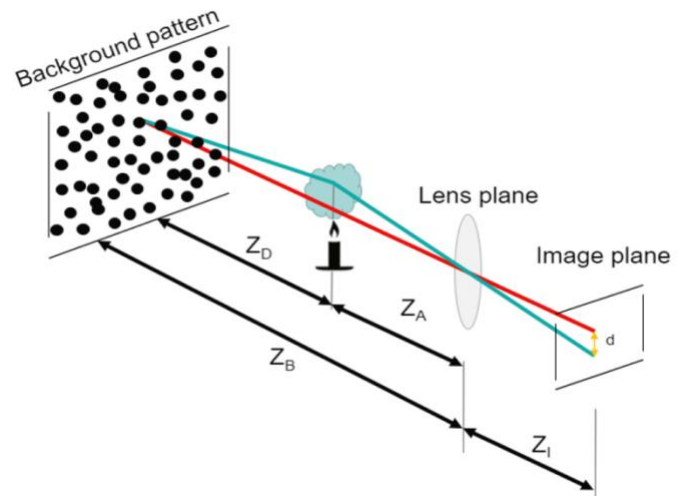


**Figure 13.** Working principle of BOS. The steady background pattern appears distorted when observed through an optical inhomogeneous media and by comparing the distorted image (blue line) with an undistorted image (red line) of the target the apparent local displacement ( $d$ ) of the background pattern can be measured.

### 5. DETAILED BLOWDOWN MODELLING

Having defined the specification of the key components for the rig, namely the CO<sub>2</sub> charge, HP and LP tank volumes, and nozzle geometry, this section is focussed on evaluating the range of possible test conditions that the rig can achieve. To do this, the transient lumped-mass blowdown model is coupled to the quasi-steady nozzle model and the blowdown process is simulated for a range of target test section inlet stagnation conditions, denoted as  $P_0$  and  $T_0$ . The range of target inlet conditions are depicted in Figure 14 in the temperature-entropy ( $T-s$ ) and temperature-pressure ( $T-P$ ) planes by the black dots, and these correspond to possible inlet conditions for a sCO<sub>2</sub> compressor operating near the critical point. In these plots, the contours report the corresponding vapour quality at the nozzle throat, assuming that the nozzle is choked, and this is calculated under the assumption of thermal and mechanical phase equilibrium. For example, for an expansion from a stagnation inlet condition of 70 bar and 30 °C, the expected vapour quality at the choked throat conditions would be 80%. Ultimately, this figure is useful to assess the range of stagnation conditions for which condensation may be expected.

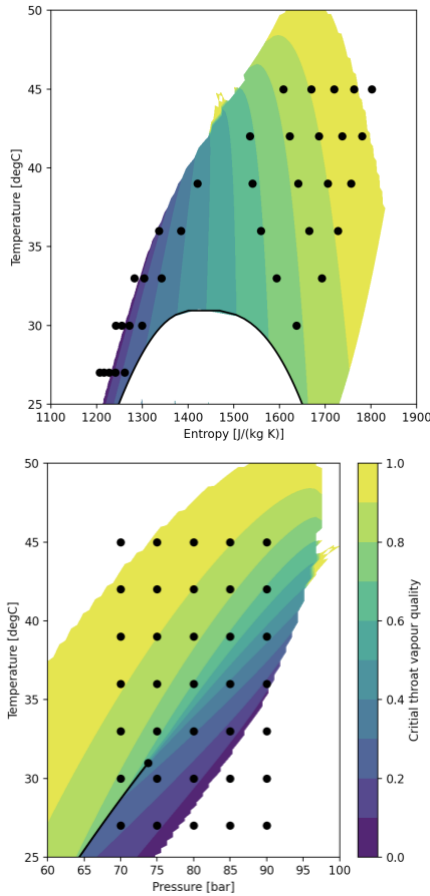


**FIGURE 14:** Vapour quality at choked flow condition for expansion from different stagnation inlet conditions.

For each target stagnation test section inlet condition, the blowdown model is run to assess the achievable blowdown time, and to assess the expected variation in the flow conditions within the nozzle during the blowdown process. As noted previously, a pressure regulating valve is installed between the HP tank and the nozzle test section that maintains a constant pressure at the inlet to the test section. In this context, the achievable blowdown time is defined as the time for which a constant stagnation inlet pressure to the test section can be achieved. Moreover, it is evident that the initial pressure in the HP tank must be higher than the target pressure. Therefore, it is necessary to determine the initial HP conditions that will provide the longest blowdown time. A higher initial HP tank pressure will provide a constant pressure for a longer period; however, the corresponding HP tank temperature will have to increase. Thus, it is beneficial to increase as much as possible, whilst not exceeding the maximum rated pressure and temperature and the HP tank, referred to as  $P_{\max}$  and  $T_{\max}$  respectively. To determine the optimal conditions, the first step is to determine the target test section inlet enthalpy, namely  $h_0 = f(T_0, P_0)$ . The expansion across the pressure regulating valve is modelled as an isenthalpic expansion and thus the corresponding HP tank temperature if  $P_{\text{HP}} = P_{\max}$  can be found since  $T_{\text{HP}} = f(P_{\text{HP}}, h_0)$ . If  $T_{\text{HP}} < T_{\max}$ , then the target test conditions can be

achieved whilst expanding from the maximum pressure. Otherwise,  $P_{\text{HP}}$  must be reduced and this is found from  $P_{\text{HP}} = f(T_{\max}, h_0)$ . Once the HP conditions are known, the LP tank conditions can be determined from the known charge, and assuming the LP tank starts at thermal equilibrium with the ambient surroundings. With the initial HP and LP conditions known, the simulation of the blowdown process can then proceed, and the achievable blowdown time can be assessed. The results obtained for the grid of target test section inlet conditions defined in figure 14, are reported in figure 15. As noted, this corresponds to the achievable blowdown time whilst maintaining a constant stagnation pressure at the inlet to the test section. Ultimately, it is observed that for expansions that are initiated from inlet conditions that sit on the right side of the critical point as viewed in the  $T$ - $s$  diagram (i.e., condensing flows), blowdown times in the order of a few seconds are expected to be possible. For inlet conditions that sit on the left side of the critical point (i.e., cavitating flows) the blowdown time reduces to less than a second. This reduction in blowdown time can be attributed to the higher upstream densities on the left side of the critical point compared to those on the right, that leads to a more rapid mass-transfer between the tanks, and a more rapid pressurisation and depressurisation of the LP and HP tanks respectively. Whilst these blowdown times are short, they are consistent with those studied in other blowdown tests of other non-ideal working fluids, such as those detailed in [8] and [9].

Finally, it should be noted that these results are obtained based on a simple model for the pressure regulating valve that assumes an isenthalpic expansion, whilst the nozzle is modelled assuming quasi-steady flow. A dynamic model of the entire test line is currently under development, which will allow the dynamics of the valve to be included in the blowdown model, and will also account for the transient nature of the flow inside the nozzle, accounting for possible mass accumulation within different control volumes that make up the whole blowdown line. As such, these initial predictions will be further investigated in the future.

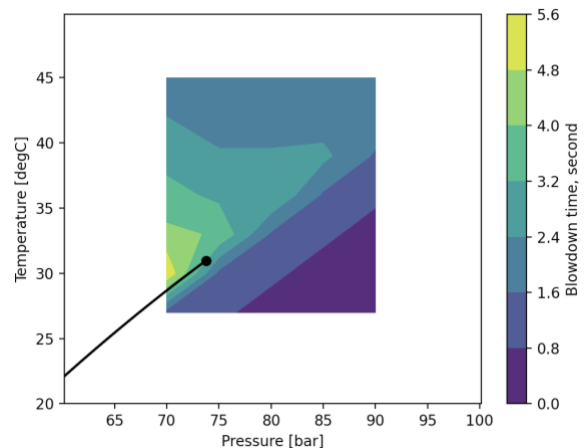


**FIGURE 15:** Achievable blowdown time whilst maintaining a constant stagnation pressure at the test section inlet for different target test section inlet pressures and temperatures.

## 6. CONCLUSION

The presented work underlines the design of a blowdown test rig to study the near dome expansion expected at the suction side of the turbocompressors for supercritical CO<sub>2</sub> cycles. The closed-loop arrangement of the test rig allows for significant savings over the direct blowdown configuration and provides the opportunity to use the test rig for higher flow rate demanding future research. Currently, the test rig is under development and manufacturing. Although experimental results are yet to be obtained, the tools used for the design of the test rig have been validated with other available data referred in the references list. The results show that achieving a constant inlet pressure to the nozzle in a range of 80 – 100 bar will be achievable upstream of the nozzle with the current design for a duration of up to five seconds which is deemed sufficient for the intended studies.

## ACKNOWLEDGEMENTS

The funding for this research has been provided by the Engineering and Physical Sciences Research Council (EPSRC) in the UK under research grant EP/V001752/1 (SCoTWoHR).

## REFERENCES

- [1] C. Forman, I. K. Muritala, R. Pardemann and B. Meyer, “Estimating the global waste heat potential,” *Renewable and Sustainable Energy Reviews*, vol. 57, p. 1568–1579, 2016.
- [2] M. Marchionni, G. Bianchi and S. A. Tassou, “Review of Supercritical Carbon Dioxide (SCO<sub>2</sub>) Technologies for High-Grade Waste Heat to Power Conversion,” *SN Applied Sciences*, p. 1–13, 2020.
- [3] M. Biondi, A. Giovannelli, G. Di Lorenzo and C. Salvini, “Techno-economic analysis of a sCO<sub>2</sub> power plant for waste heat recovery in steel industry,” *Energy Reports*, vol. 6, pp. 298–304, 2020.
- [4] M. Marchionni, G. Bianchi and S. A. Tassou, “Techno-Economic Assessment of Joule-Brayton Cycle Architectures for Heat to Power Conversion from High-Grade Heat Sources Using CO<sub>2</sub> in the Supercritical State,” *Energy*, p. 1140–1152, 2018.
- [5] G. Persico, P. Gaetani, A. Romei, L. Toni, E. F. Bellobuono and R. Valente, “Implications of phase change on the aerodynamics of centrifugal compressors for supercritical carbon dioxide applications,” *Journal of Engineering for Gas Turbines and Power*, vol. 143, no. 4, p. 041007, 2021.
- [6] A. Ameli, A. Afzalifar, T. Turunen-Saaresti and J. Backman, “Effects of real gas model accuracy and operating conditions on supercritical CO<sub>2</sub> compressor performance and flow field,” *Journal of Engineering for Gas Turbines and Power*, vol. 140, no. 6, p. 062603, 2018.
- [7] A. Ameli, T. Turunen-Saaresti and J. Backman, “Numerical investigation of the flow behavior inside a supercritical CO<sub>2</sub> centrifugal compressor,” *Journal of Engineering for Gas Turbines and Power*, vol. 140, no. 12, p. 122604, 2018.
- [8] N. D. Baltadjiev, C. Lettieri and Z. S. Spakovszky, “An Investigation of Real Gas Effects in Supercritical CO<sub>2</sub> Centrifugal Compressors,” *Journal of Turbomachinery*, p. 137, 2015.
- [9] C. Lettieri, D. Paxson, Z. Spakovszky and P. Bryanston-Cross, “Characterization of Nonequilibrium Condensation of Supercritical Carbon Dioxide in a de Laval Nozzle,” *Journal of Engineering for Gas Turbines and Power*, p. 140, 2018.
- [10] C. Lettieri, D. Yang and Z. Spakovszky, “An investigation of condensation effects in supercritical carbon dioxide compressors,” *Journal of Engineering for Gas Turbines and Power*, vol. 137, no. 8, p. 082602, 2015.
- [11] A. Romei and G. Persico, “Computational fluid-dynamic modelling of two-phase compressible flows of carbon dioxide in supercritical conditions,” *Applied Thermal Engineering*, vol. 190, p. 116816, 2021.
- [12] A. Romei, P. Gaetani and G. Persico, “Computational fluid-dynamic investigation of a centrifugal compressor with inlet guide vanes for supercritical carbon dioxide power systems,” *Energy*, vol. 255, p. 124469, 2022.
- [13] G. Petruccelli, T. Turunen-Saaresti, A. Grönman and A. Lugo, “Study on the Operation of the LUTsCO<sub>2</sub> Test Loop with Pure CO<sub>2</sub> and CO<sub>2</sub>+ SO<sub>2</sub> Mixture Through Dynamic Modeling,” in *International Seminar on Non-Ideal Compressible-Fluid Dynamics for Propulsion & Power*, London, 2022.
- [14] M. C. Robertson, P. J. Newton, T. Chen and R. F. Martinez-Botas, “Development and commissioning of a blowdown facility for dense gas vapours,” in *In Turbo Expo: Power for Land, Sea, and Air*, Phoenix, 2019.
- [15] M. White, “Investigating the wet-to-dry expansion of organic fluids for power generation,” *International Journal of Heat and Mass Transfer*, vol. 192, p. 122921, 2021.
- [16] W. D. Seider, D. R. Lewin, J. D. Seader, S. Widagdo, R. Gani and K. M. Ng, *Product and process design principles: synthesis, analysis, and evaluation*, New York: John Wiley & Sons, 2017.
- [17] B. HSE, *EH40/2005 Workplace exposure limits*, 4th Edition, London: The Stationery Office, 2020.
- [18] M. White and A. Sayma, “Design of a closed-loop optical-access supersonic test facility for organic vapours,” in *ASME Turbo Expo, GT2018*, Oslo, 2018.
- [19] D. E. Paxson, “Experimental characterization of condensation behavior for metastable carbon dioxide, PhD diss.,” Massachusetts Institute of Technology, 2016.
- [20] J. M. Cullen and J. M. Allwood, “Theoretical Efficiency Limits for Energy Conversion Devices,” *Energy*, p. 2059–2069, 2010.